

# Subspace Optimization for Backpropagation-Free Continual Test-Time Adaptation

Damian Sójka<sup>1,2</sup> (✉), Sebastian Cygert<sup>3,4</sup>, and Marc Masana<sup>5</sup>

<sup>1</sup> Poznan University of Technology <sup>2</sup> IDEAS NCBR

<sup>3</sup> NASK - National Research Institute <sup>4</sup> Gdańsk University of Technology

<sup>5</sup> Graz University of Technology

damian.sojka@doctorate.put.poznan.pl

**Abstract.** We introduce PACE, a backpropagation-free continual test-time adaptation system that directly optimizes the affine parameters of normalization layers. Existing derivative-free approaches struggle to balance runtime efficiency with learning capacity, as they either restrict updates to input prompts or require continuous, resource-intensive adaptation regardless of domain stability. To address these limitations, PACE leverages the Covariance Matrix Adaptation Evolution Strategy with the Fastfood projection to optimize high-dimensional affine parameters within a low-dimensional subspace, leading to superior adaptive performance. Furthermore, we enhance the runtime efficiency by incorporating an adaptation stopping criterion and a domain-specialized vector bank to eliminate redundant computation. Our framework<sup>1</sup> achieves state-of-the-art accuracy across multiple benchmarks under continual distribution shifts, reducing runtime by over 50% compared to existing backpropagation-free methods.

## 1 Introduction

Test-time adaptation (TTA) [31] has emerged as a practical approach to adapt a deployed neural networks on-the-fly, increasing its robustness to shifting data distributions. While backpropagation (BP)-based methods [22, 23, 31, 32] achieve strong performance via self-supervised learning, their high memory requirements and incompatibility with non-differentiable quantized models limit their deployment on resource-constrained edge devices [4, 15, 21]. Conversely, although existing BP-free methods reduce memory overhead and support quantization [1, 4, 14, 21], the inherent challenges of derivative-free adaptation hinder their ability to balance runtime efficiency with learning capacity (Fig. 1).

Existing BP-free methods suffer from two primary limitations: 1) restricted learning capacity: current state-of-the-art does not update the model parameters [1, 14, 16, 18, 25], limits updates to input prompts [21], or relies on inherently noisy zeroth-order gradient estimation [4, 26], which limits their ability to resolve complex distribution shifts. 2) high computational overhead: existing

---

<sup>1</sup> Code available at <https://github.com/dmn-sjk/PACE.git>. Pre-print.

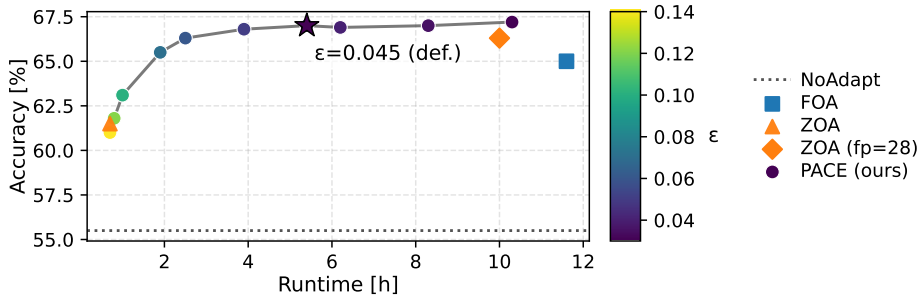


**Fig. 1. Accuracy versus runtime trade-off** on the ImageNet-C benchmark using a ViT-B model, across various adaptation stopping thresholds  $\epsilon$  (star marks the default setting  $\epsilon=0.045$ ). The horizontal dotted line represents the NoAdapt baseline accuracy. Existing BP-free methods typically face a trade-off: they either achieve high accuracy at the expense of computational efficiency or reduce runtime by sacrificing precision. Our approach not only outperforms current baselines but also introduces a tunable mechanism to balance the accuracy-runtime trade-off, preventing the inefficient use of resources for diminishing returns.

approaches [4, 21] require numerous forward passes to match the performance of BP-based methods. Furthermore, these methods waste resources by performing adaptation on every batch indefinitely, regardless of domain stability.

To address these challenges in TTA, we introduce Projected Adaptation via Covariance Evolution (PACE), an efficient BP-free adaptation system that expands learning capabilities while minimizing inference overhead.

We start by adapting the model utilizing the Covariance Matrix Adaptation Evolution Strategy (CMA-ES), since its effectiveness for TTA was already confirmed [21]. The high dimensionality of neural network weights makes direct CMA-ES optimization intractable. To circumvent this, [21] focuses on updating input prompts rather than internal weights. However, our experiments demonstrate that input prompt tuning is significantly inferior to updating the affine parameters of normalization layers (Fig. 2), as commonly done in TTA [22, 23, 31]. While this finding motivates the application of CMA-ES directly to the normalization layers to maximize adaptation capability, doing so naively remains computationally intractable due to the high-dimensional nature of these parameters. Therefore, we exploit the observation of low intrinsic dimensionality for TTA gradients [7], a property we verify empirically in Fig. 3. PACE optimizes a low-dimensional vector and projects it into the high-dimensional normalization weight space via the Fastfood transform [17], enabling highly effective adaptation without backpropagation.

Furthermore, we observe that the CMA-ES adaptation predominantly occurs at the onset of a stable domain, yielding negligible accuracy improvements in later batches (Fig. 4). We leverage this by designing a dynamic stopping criterion based on the mean shift of the CMA-ES distribution. Once adaptation halts, the model operates with almost zero computational overhead. When a domain shift

is detected, adaptation automatically resumes. Finally, to accumulate knowledge across domain shifts, we maintain a bank of domain-specialized adaptation vectors, allowing the system to rapidly recover performance when encountering repeated domains. These components combine to form a fully practical TTA system, especially suitable for long-term deployment.

In summary, our contributions are:

- We develop PACE, a BP-free continual TTA method that efficiently optimizes normalization layers using CMA-ES, utilizing Fastfood transform projections to search a low-dimensional subspace.
- We introduce a dynamic stopping criterion based on the CMA-ES distribution mean that halts adaptation during stable domain phases, eliminating computational overhead.
- We integrate a domain-specialized vector bank, enabling the model to accumulate knowledge and rapidly adapt to recurring domains.

These lead to our proposed method outperforming the best BP-free approaches in both efficiency and accuracy, achieving around 50% reduction in runtime. Noticeably, PACE significantly surpasses the other CMA-ES-based method (FOA).

## 2 Related Work

**Test-Time Adaptation.** TTA targets distribution shifts during inference by adapting pre-trained models without access to source data or labels [31]. Continual TTA further assumes a non-stationary environment where domains change without access to domain labels [32]. Existing methods can be divided into backpropagation-based (BP-based) and backpropagation-free (BP-free).

**BP-based methods.** These methods utilize gradient descent to update model parameters at test time. To balance efficiency with learning capacity, most approaches restrict updates to affine parameters in normalization layers [5, 22, 23, 31]. In the absence of labels, these methods employ self-supervised objectives such as entropy minimization [22, 28, 31], pseudo-labeling variants [5, 32], rotation prediction [27], or feature distribution alignment [19]. Because self-supervised signals can be unreliable, stabilization techniques are often required. For instance, SAR [23] filters samples by entropy and seeks flat loss minima, while CoTTA [32] adopts a teacher-student framework with stochastic weight restoration. Despite their effectiveness, BP-based methods demand high memory and differentiable weights, which limits their utility on quantized or resource-constrained edge devices.

**BP-free methods.** Early BP-free TTA focused on adjusting batch normalization statistics using test data batches [8, 20, 25]. Subsequent work extended the statistics update to single-sample adaptation [16] and handling the temporal class correlation [8, 36]. However, these approaches require the presence of batch normalization layers in model architectures. Further works explored prototype-based classifier adjustment (T3A) [14] and logits correction (LAME) [1]. None

of those methods update core model weights, resulting in significantly limited learning capacity. Recent work introduces weight-updating BP-free methods: FOA [21] adapts input prompts via CMA-ES, and ZOA [4] employs zeroth-order gradient estimation. While promising, FOA’s prompt-only updates restrict its flexibility. Furthermore, FOA adapts on every batch, demanding up to 28 forward passes, which is computationally prohibitive for every data sample in real-world deployment. In contrast, ZOA reliably updates core model weights with only 2 forward passes. However, to remain competitive with BP-based methods, its computational demands are similar to FOA. Our PACE improves adaptation effectiveness through subspace adaptation of affine parameters of normalization layers via CMA-ES and minimizes overhead by introducing an automated stopping criterion that halts adaptation once it is no longer beneficial. Additionally, drawing on recent BP-based TTA work [30], we incorporate a domain-specialized vector bank to aggregate knowledge across diverse environments. This mechanism enables the model to rapidly recover performance when re-encountering domains, significantly enhancing its readiness for practical deployment.

### 3 Problem Statement

Continual TTA consists of adapting a pre-trained source model  $f_{\theta^{(0)}}$  to a non-stationary sequence of unlabeled domains. The model is initially trained on a labeled source dataset  $\mathcal{D}_s = \{(\mathbf{x}_i, \mathbf{y}_i)\}_{i=1}^{N_s}$  sampled from distribution  $\mathcal{P}_s$ . At inference, the model encounters a sequence of  $T$  domains:

$$\mathcal{D}_t^{(1)}, \dots, \mathcal{D}_t^{(T)} \quad \text{where} \quad \mathcal{D}_t^{(k)} = \{\mathbf{x}_j^{(k)}\}_{j=1}^{N_k}, \quad \mathbf{x}_j^{(k)} \sim \mathcal{Q}^{(k)}(\mathbf{x}). \quad (1)$$

Each domain  $\mathcal{D}_t^{(k)}$  consists of unlabeled samples  $\{\mathbf{x}_j^{(k)}\}$ . These domains are out-of-distribution ( $\mathcal{Q}^{(k)} \neq \mathcal{P}_s$ ) and the sequence is non-stationary ( $\mathcal{Q}^{(k)} \neq \mathcal{Q}^{(k+1)}$ ). The model is adapted on-the-fly using only current samples.

## 4 Methodology

We introduce a novel BP-free continual TTA method, named Projected Adaptation via Covariance Evolution (PACE), designed to be a fully practical TTA system. It comprises three main components: Subspace Adaptation 4.1, Adaptation Stopping 4.2, and Domain-Specialized Vector Bank 4.3. The diagram of our proposed PACE method is presented at the end of this section (Fig. 5).

### 4.1 Subspace Adaptation

Building on established TTA frameworks [5, 22, 23, 31] and our observation that input prompt tuning is less effective than updating affine parameters of normalization layers (Fig. 2), we employ CMA-ES to optimize these layers. To ensure high-dimensional optimization remains tractable by CMA-ES, we leverage the

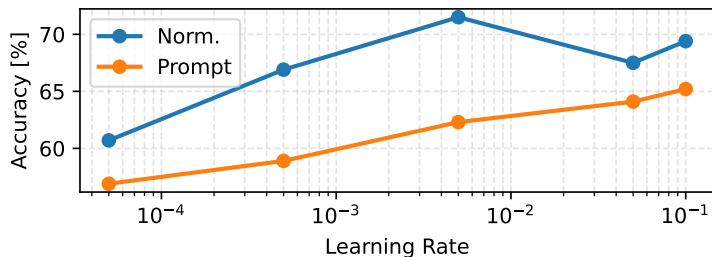


**Fig. 2. Observed performance gap.** A comparison of updating the affine parameters of normalization layers (NORM.) versus three input prompts (PROMPT) for a ViT-B model during test-time adaptation on ImageNet-C. We adapt these using ground-truth labels with an SGD optimizer with varying learning rate. Updating the normalization layers allows the model to more effectively ‘correct’ the covariate shift at each network depth for all reported learning rate values.

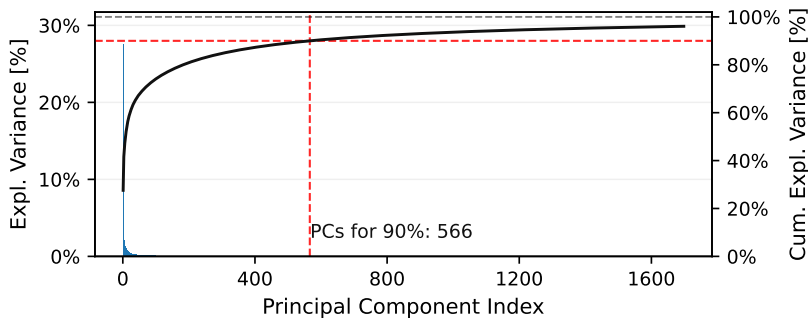


**Fig. 3. Intrinsic dimensionality of continual TTA gradients.** The affine parameters of normalization layers from a ViT-B model are optimized via SGD with the loss function from FOA [21]. The concatenated gradients from all ImageNet-C domains reveal that only 566 components explain 90% of the variance. This highlights the low-dimensional nature of the adaptation space. Note that only the most significant components are shown for clarity. The analysis is based on 11 729 gradient batches.

observation that TTA gradients have low intrinsic dimensionality (as noted in [7] and shown in Fig. 3), which suggests that effective updates can be achieved within a low-dimensional subspace. This was also noticed by Duan et al. [7], using a few batches from a single domain. We extend this observation to all concatenated domains, where the major directions are still low despite the domain changes.

**Model update.** We adapt the model weights by adding the constant random projection  $\text{proj}(\cdot)$  of a low-dimensional vector  $\mathbf{v} \in \mathbb{R}^d$  into a high-dimensional space  $\text{proj}(\mathbf{v}) \in \mathbb{R}^D$ , where  $D \gg d$ . The adapted model weights are the affine parameters of normalization layers, therefore we set  $D$  to be equal to their total dimensionality. We partition  $\text{proj}(\mathbf{v})$  to match the dimensionality of each param-

eter tensor and add the resulting components to the initial weights to get the adapted model  $f_{\boldsymbol{\theta}^{(0)}+\text{proj}(\mathbf{v})}$ . Initializing with a zero vector ( $\mathbf{v} = \mathbf{0}$ ) ensures the adaptation starts exactly from the state of the pre-trained model. Our adaptation objective is to find the optimal low-dimensional vector  $\mathbf{v}^*$  that minimizes the fitness function  $\mathcal{L}(\cdot)$  given test samples  $\mathbf{x}$ :

$$\mathbf{v}^* = \underset{\mathbf{v}}{\operatorname{argmin}} \mathcal{L}(f_{\boldsymbol{\theta}^{(0)}+\text{proj}(\mathbf{v})}(\mathbf{x})). \quad (2)$$

**CMA-ES optimization.** We propose to perform the adaptation using the CMA-ES strategy. Rather than directly optimizing the vector  $\mathbf{v}$ , CMA-ES maintains and optimizes a multivariate Gaussian distribution over the search space. At each iteration  $t$  ( $t$ -th test batch), a population of  $K$  candidate solutions is sampled from this distribution:

$$\mathbf{v}_k^{(t)} \sim \mathbf{m}^{(t)} + \tau^{(t)} \mathcal{N}(\mathbf{0}, \boldsymbol{\Sigma}^{(t)}), \quad (3)$$

where  $k = 1, \dots, K$ . Here,  $\mathbf{m}^{(t)} \in \mathbb{R}^d$  represents the mean of the search distribution at iteration step  $t$ ,  $\tau^{(t)} \in \mathbb{R}^+$  is the overall standard deviation controlling the global step size, and  $\boldsymbol{\Sigma}^{(t)}$  is the covariance matrix defining the distribution's shape and orientation.

For each candidate  $\mathbf{v}_k^{(t)}$ , we evaluate its fitness by updating the model and computing the loss on the current test sample  $\mathbf{x}^{(t)}$ . This yields a fitness value  $l_k$  for each candidate. CMA-ES then updates the distribution parameters ( $\mathbf{m}^{(t)}$ ,  $\tau^{(t)}$ , and  $\boldsymbol{\Sigma}^{(t)}$ ) for the next generation based on the ranking of the fitness values. This process systematically increases the likelihood of previously successful candidates (see [9] for details). Following [21], we output the prediction associated with the lowest fitness value as the final prediction of the model.

**Fitness function.** We utilize the fitness function used in FOA [21] and ZOA [4] due to its proven effectiveness, and to enable direct comparison. Prior to adaptation, we pass a small set of source data through the model to calculate the means and standard deviations of activations from  $L$  intermediate model blocks, denoted as  $\{\mu_{s,i}, \sigma_{s,i}\}_{i=1}^L$ . During test time, we calculate the corresponding statistics on the current batch of test samples  $\mathbf{x}^{(t)}$ , yielding  $\{\mu_i(\mathbf{x}^{(t)}), \sigma_i(\mathbf{x}^{(t)})\}_{i=1}^L$ . The fitness function combines the prediction entropy with the difference between these activation statistics:

$$\begin{aligned} \mathcal{L}(f_{\boldsymbol{\theta}^{(0)}+\text{proj}(\mathbf{v}_k^{(t)})}(\mathbf{x}^{(t)})) &= \frac{1}{B \times C} \sum_{\mathbf{x} \in \mathbf{x}_t} \sum_{c=1}^C -y_c \log y_c \\ &+ \lambda \sum_{i=1}^L \left( \|\mu_i(\mathbf{x}^{(t)}) - \mu_{s,i}\|_2 + \|\sigma_i(\mathbf{x}^{(t)}) - \sigma_{s,i}\|_2 \right) \end{aligned} \quad (4)$$

where  $B$  is the batch size,  $C$  is the total number of classes,  $y_c$  is the  $c$ -th element of the prediction probability vector  $\hat{\mathbf{y}} = f_{\boldsymbol{\theta}^{(0)}+\text{proj}(\mathbf{v}_k^{(t)})}(\mathbf{x}^{(t)})$ , and  $\lambda$  is a balancing hyperparameter.

**Efficient dimensionality expansion.** To efficiently project low-dimensional vectors  $\mathbf{v}$  into the high-dimensional parameter space, we employ the Fastfood transform [17]. Standard dimensionality expansion requires multiplying  $\mathbf{v}$  by a dense projection matrix  $\mathbf{W} \in \mathbb{R}^{D \times d}$ . Storing this dense matrix can incur high memory costs for large networks. Fastfood circumvents this bottleneck by approximating the dense Gaussian matrix  $\mathbf{W}$  with a product of structured diagonal matrices and the Fast Walsh-Hadamard Transform (FWHT). We redefine the linear projection as:

$$\mathbf{W}\mathbf{v} \approx \mathbf{S}\mathbf{H}\mathbf{G}\mathbf{P}\mathbf{H}\mathbf{B}\mathbf{v} = \text{proj}(\mathbf{v}), \quad (5)$$

where  $\mathbf{B} \in \mathbb{R}^{d \times d}$  is a diagonal matrix with entries sampled uniformly from  $\{-1, 1\}$ ,  $\mathbf{P} \in \mathbb{R}^{D \times D}$  is a random permutation matrix, and  $\mathbf{G} \in \mathbb{R}^{D \times D}$  is a diagonal matrix with entries drawn from a standard normal distribution  $\mathcal{N}(0, 1)$ . The matrix  $\mathbf{S} \in \mathbb{R}^{D \times D}$  is a diagonal scaling matrix ensuring the rows of the resulting pseudo-random matrix possess the correct  $L_2$  norm to approximate the  $\chi$ -distribution of a true Gaussian random matrix. Finally,  $\mathbf{H}$  represents the Walsh-Hadamard matrix. We perform multiplication by  $\mathbf{H}$  via the FWHT, entirely avoiding the instantiation of the matrix in memory.

To achieve the exact target dimensionality  $D$ , we pad the input to the nearest power of two (enabling FWHT), process it through stacked independent Fastfood blocks, and subsequently slice it to the required length. We initialize the Fastfood transform components once at the beginning of the adaptation phase and freeze them for the remainder of the process.

By default, we set  $d = 2304$  and the dimensionality of the updated ViT-B model parameters is equal to  $D = 34800$ . In that case, the Fastfood transform significantly reduces memory overhead, requiring only 0.13 MB compared to the 306 MB needed for a standard dense projection matrix.

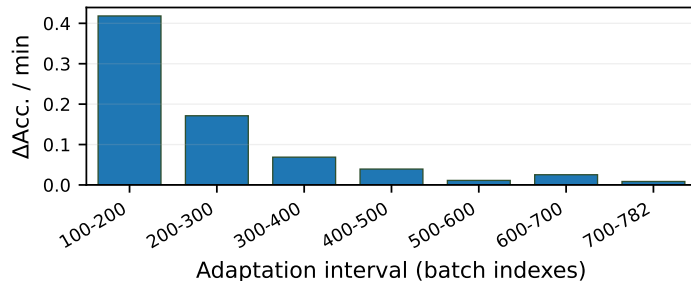


**Fig. 4. Marginal accuracy gain per unit time** across adaptation budgets on ImageNet-C with ViT-B model. For each consecutive pair of adaptation step budgets, we compute the increase in mean accuracy across domains and divide it by the additional estimated wall-clock time required for that interval using our Subspace Adaptation with CMA-ES algorithm. The mean of CMA-ES distribution  $\mathbf{m}$  is used as the evaluated model update. Higher bars indicate more efficient use of adaptation time, while decreasing bars indicate diminishing returns from further adaptation.

## 4.2 Adaptation Stopping

We observe that adaptation at the beginning of a stable domain drives the majority of performance improvements (Fig. 4). However, the adaptation process incurs significant computational overhead. While test data distributions might remain stable for extended periods in real-world deployment, current BP-free TTA methods adapt indefinitely. This approach wastes computational resources and energy, a critical bottleneck for long-term deployments on embedded devices. To address this inefficiency, we introduce a heuristic to halt adaptation when it yields marginal performance gains.

**Stopping heuristic.** CMA-ES continuously updates its distribution to track optimal candidates. Therefore, we monitor the relative change in distribution mean  $\mathbf{m}$ . Specifically, we stop the adaptation when the normalized difference between the distribution mean at the current time step  $\mathbf{m}^{(t)}$  and the previous time step  $\mathbf{m}^{(t-1)}$  falls below a convergence threshold  $\epsilon$ :

$$\frac{\|\mathbf{m}^{(t)} - \mathbf{m}^{(t-1)}\|}{\|\mathbf{m}^{(t-1)}\|} < \epsilon. \quad (6)$$

We rely on this specific formulation because the mean  $\mathbf{m}^{(t)}$  represents the algorithm’s current best estimate for the optimal parameters  $\mathbf{v}$ . When this relative change approaches zero, it indicates that the CMA-ES optimization has converged to a local optimum for the current data distribution. Furthermore, normalizing the difference by the previous mean ensures that our stopping criterion is scale-invariant, making it robust across different network layers or parameter magnitudes. Once the stopping criterion in Eq. 6 is satisfied, the model is updated with the CMA-ES mean  $\mathbf{m}^{(t)}$  and fixed.

**Resuming the adaptation.** Since continual TTA lacks explicit domain labels, we require a criterion to re-initialize the adaptation process. To detect these shifts, we adopt the domain shift detection scheme established in [2, 4, 13], which remains invariant to updates to the model.

We maintain the exponential moving average (EMA) of the activation statistics from the stem layer of the model:

$$\phi_{EMA}^{(t-1)} = \beta\phi^{(t-1)} + (1 - \beta)\phi_{EMA}^{(t-2)}, \quad (7)$$

where  $\phi^{(t-1)}$  represents the activation mean and variance for the  $(t-1)$ -th batch, and  $\beta = 0.8$  denotes the moving average factor. To quantify the shift  $U$ , we compute the symmetric Kullback-Leibler (KL) divergence between the current batch statistics  $\phi^{(t)}$  and the historical EMA  $\phi_{EMA}^{(t-1)}$ :

$$U(\phi_{EMA}^{(t-1)}, \phi^{(t)}) = \frac{1}{H} \sum_{i=1}^H [KL(\phi_{EMA}^{(t-1),i} \parallel \phi^{(t),i}) + KL(\phi^{(t),i} \parallel \phi_{EMA}^{(t-1),i})], \quad (8)$$

where  $H$  is the dimensionality of the statistics. A domain shift is detected when this distance exceeds a predefined threshold  $\gamma$ , at which point we re-initialize

the adaptation using the Domain-Specialized Vector Bank. To ensure robust detection, we cease updating  $\phi_{EMA}$  once the adaptation has stopped, by the technique described above.

### 4.3 Domain-Specialized Vector Bank

In real-world, long-term deployments, domain recurrence can be a common phenomenon [30]. A fully practical TTA system must account for this by rapidly reusing knowledge acquired from previously encountered domains.

To achieve this, we maintain a memory bank  $\mathcal{B}$  of vectors  $\mathbf{v}$  derived from past domains. Specifically, upon detecting a domain shift, we archive the current mean of the CMA-ES search distribution,  $\mathbf{m}$ , into the bank. For the incoming domain, the new CMA-ES optimizer is initialized using the archived mean that minimizes the fitness function  $\mathcal{L}$  on the current data batch  $\mathbf{x}^{(t)}$ :

$$\mathbf{m}_{init} = \arg \min_{\mathbf{m}_i \in \mathcal{B}} \mathcal{L}(f_{\theta^{(0)} + \text{proj}(\mathbf{m}_i)}(\mathbf{x}^{(t)})). \quad (9)$$

Adaptation then proceeds conventionally. This retrieval mechanism facilitates the rapid reuse of learned experiences, effectively preventing performance degradation even in the presence of sudden domain shifts.

To ensure strict memory bounds, we constrain the maximum capacity of the bank to  $p$  vectors. When a newly optimized mean is added to a full bank ( $|\mathcal{B}| > p$ ), we employ a redundancy-based removal policy. We calculate the average pairwise cosine similarity for each mean  $\mathbf{m}_i$  in the bank and discard the vector that exhibits the highest average similarity to the others:

$$\mathbf{m}_{drop} = \arg \max_{\mathbf{m}_i \in \mathcal{B}} \frac{1}{|\mathcal{B}| - 1} \sum_{\mathbf{m}_j \in \mathcal{B} \setminus \{\mathbf{m}_i\}} \frac{\mathbf{m}_i \cdot \mathbf{m}_j}{\|\mathbf{m}_i\| \|\mathbf{m}_j\|} \quad (10)$$

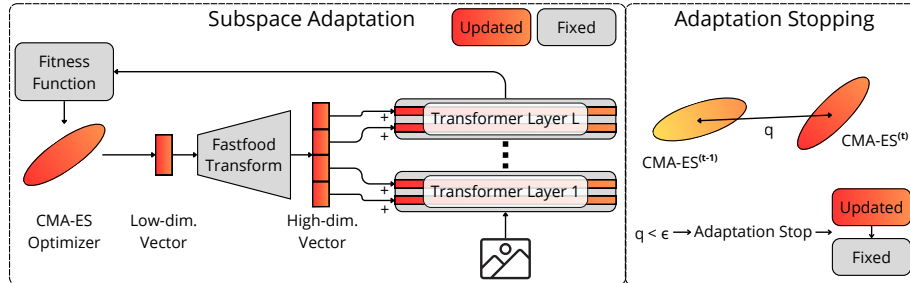


**Fig. 5. Diagram of PACE.** 1) **Subspace Adaptation:** we adapt the model by adding a high-dimensional random projection of a small, learnable vector to the model’s normalization layer weights. We use the CMA-ES strategy to iteratively evolve a population of these vectors, selecting the one that minimizes the loss on current test samples. 2) **Adaptation Stopping:** for efficiency, we stop the adaptation when the mean of the distribution optimized by CMA-ES is lower than a threshold. Along with the **Domain-Specialized Vector Bank**, they make an effective and efficient TTA system.

This strategy effectively prunes the most redundant information, maximizing the diversity of the domain representations stored in the bank.

Subspace adaptation enables memory-efficient storage of knowledge from previous domains. A single `float32` domain vector with our default dimensionality ( $d=2304$ ) occupies approximately 0.0088 MB of memory. Consequently, the total memory usage is only about 0.26 MB when the bank’s maximum default capacity  $p=30$  is utilized.

## 5 Experiments

**Datasets and models.** We conduct experiments on three standard TTA benchmarks: ImageNet-C [11], ImageNet-R [10], and DomainNet-126 [24]. ImageNet-C consists of 15 corruption functions across five severity levels. Following the protocol in [32], we evaluate using the classic corruption sequence with the highest severity level. ImageNet-R provides diverse renditions of 200 ImageNet classes, while DomainNet-126 contains images from four distinct domains (real, clipart, painting, and sketch).

Experiments are reported with both full-precision and quantized versions of ViT-B [6] and DeiT-B [29] models. Unless otherwise specified, experiments are reported with full-precision models. We implement quantization using PTQ4ViT [34], following [21]. For ImageNet benchmarks, we use checkpoints trained on the ImageNet-1K [3] training set obtained from the `timm` repository [33]. For DomainNet-126, we utilize models trained on the *real* domain using the repository from [35] and evaluate on the remaining three domains.

**Baselines.** We compare against both previously defined categories of state-of-the-art TTA methods: BP-free, including LAME [1], T3A [14], FOA [21], and ZOA [4], and BP-based, specifically TENT [31], CoTTA [32], and SAR [23]. To ensure a fair comparison, we also compare with ZOA (fp=28), a modified version of ZOA where we match the number of forward passes used in FOA and PACE by increasing the sampled perturbations for gradient estimation to 27. Finally, NoAdapt represents the fixed source model without adaptation.

**Implementation details.** For all experiments, we maintain a batch size of 64 to ensure consistency with prior work [4, 21, 32]. We adopt the hyperparameter settings specified in the original papers for all baselines. In the instances where they were not provided, the learning rate was specifically tuned for the corresponding experimental setup and model. For fairness, we configure the CMA-ES population size  $K$  of FOA to 28 and set the optimization vector dimensionality  $d$  to 2304. Following both FOA and ZOA, we use the validation set of ImageNet-1K to compute the statistics of ID data and set the  $\lambda$  to 0.2 for ImageNet-R and 0.4 for all other benchmarks. We set the domain shift detection threshold  $\gamma$  to 0.03, the adaptation stopping threshold  $\epsilon$  is set to 0.045 and the maximum capacity of domain-specialized vector buffer  $p$  to 30. PACE specifically updates the affine parameters of the normalization layers.

Further details and hyperparameter ablation studies are provided in the Appendix (Sec. A.2 and Sec. A.3.1, respectively).

**Table 1.** Accuracy on ImageNet-C (IN-C), ImageNet-R (IN-R) and DomainNet-126 (DN-126) with ViT-B and DeiT-B. **Bold** indicates best result, underlined second best.

Method	Backprop.	ViT-B			DeiT-B			Avg.
		IN-C	IN-R	DN-126	IN-C	IN-R	DN-126	
NoAdapt	✗	55.5	59.5	53.1	51.6	52.8	60.2	55.5
TENT	✓	61.7	<u>63.9</u>	53.8	55.5	56.1	60.4	58.6
CoTTA	✓	58.4	<u>63.5</u>	<b>62.0</b>	55.4	53.0	60.4	58.8
SAR	✓	61.5	63.3	53.8	59.4	<u>57.4</u>	60.7	59.4
LAME	✗	54.1	59.0	51.6	50.9	52.5	58.9	54.5
T3A	✗	55.4	58.0	56.2	43.5	49.7	61.8	54.1
FOA	✗	65.0	63.8	56.0	61.3	56.3	63.0	60.9
ZOA	✗	61.5	60.7	55.8	56.9	53.5	62.4	58.5
ZOA (fp=28)	✗	<u>66.3</u>	62.6	56.5	<u>61.7</u>	55.8	<u>63.4</u>	<u>61.1</u>
PACE (ours)	✗	<b>67.0</b>	<b>64.5</b>	<u>57.0</u>	<b>62.7</b>	<b>59.5</b>	<b>64.3</b>	<b>62.5</b>

### 5.1 Results on Full-Precision Models

PACE achieves the highest average accuracy across all benchmarks and full-precision models, consistently outperforming other BP-free baselines (Tab. 1). Specifically, it surpasses direct competitors FOA and ZOA by 1.7 and 4.0 percentage points, respectively. When ZOA is modified to match the forward-pass budget of PACE and FOA (ZOA ( $fp=28$ )), our method maintains a 1.4 percentage point lead despite adapting to fewer batches.

While CoTTA achieves the highest accuracy on DomainNet-126 by leveraging backpropagation, it is significantly more memory-intensive than PACE (Tab. 3) and lacks support for quantized model updates. It is important to note that BP-based methods operate in a distinct category, as BP-free approaches are inherently constrained by the absence of direct gradient calculations. The fact that PACE outperforms BP-based methods on average, despite these inherent limitations, further underscores the effectiveness of our approach.

More detailed results on ImageNet-C are presented in Tab. A.2 and Fig. A.1 in the Appendix.

### 5.2 Results on Quantized Models

We evaluate our approach against BP-free baselines for adapting quantized networks on ImageNet-C benchmark, with results summarized in Tab. 2 for 8-bit and 6-bit ViT-B models. Our method consistently outperforms competing approaches across both bit widths. Notably, our 8-bit model achieves 65.0% accuracy, matching the 32-bit FOA baseline (65.0%) while significantly exceeding almost all 32-bit competitors.

The performance margin over ZOA ( $fp = 28$ ) increases as quantization becomes more aggressive, rising from 0.3 percentage points at 8-bit to 0.6 per-

**Table 2.** Corruption Accuracy (%) on ImageNet-C with **Quantized** ViT-B models.

Model Method	Noise			Blur			Weather				Digital			Avg.			
	Gauss.	Shot	Impul.	Defoc.	Glass	Motion	Zoom	Snow	Frost	Fog	Brit.	Contr.	Elas.		Pix.	JPEG	
8-bit	NoAdapt	55.8	55.8	56.5	46.7	34.7	52.1	42.5	60.8	61.4	66.7	76.9	24.6	44.7	65.8	66.7	54.1
	T3A	55.6	55.6	55.9	45.9	34.7	51.8	42.0	59.7	62.0	65.4	76.4	48.5	43.0	65.3	67.7	55.6
	FOA	60.7	61.4	61.3	57.2	51.5	59.4	51.3	68.0	67.3	72.4	80.3	63.2	57.0	72.0	69.8	63.5
	ZOA	57.9	60.6	61.4	51.2	44.6	56.6	51.8	64.6	61.8	63.6	78.1	54.5	54.4	68.7	68.3	59.7
	ZOA (fp=28)	60.4	62.6	63.3	56.8	53.6	62.1	58.5	67.2	67.0	70.4	79.4	60.8	63.7	72.2	72.2	64.7
	PACE (ours)	59.9	61.3	61.6	56.4	55.5	62.1	58.8	68.2	67.0	71.8	80.0	60.6	65.5	73.3	72.3	65.0
6-bit	NoAdapt	44.2	42.0	44.8	39.8	28.9	43.4	34.7	53.2	59.8	59.0	75.1	27.4	39.0	59.1	65.3	47.7
	T3A	42.9	40.6	42.1	31.4	25.5	40.2	31.9	48.7	58.3	58.1	73.8	27.2	36.7	58.8	65.7	43.3
	FOA	53.2	51.8	54.6	49.6	38.8	51.0	44.8	60.3	65.0	68.8	76.7	39.5	46.6	67.3	68.6	55.8
	ZOA	48.7	51.0	53.2	43.1	37.4	49.4	43.1	58.4	63.2	62.0	76.1	35.2	47.9	62.6	67.1	54.3
	ZOA (fp=28)	52.6	54.6	55.8	49.0	48.5	54.3	51.4	60.5	62.7	64.7	76.4	38.6	57.3	66.6	69.5	57.5
	PACE (ours)	53.2	53.9	55.0	49.2	48.6	55.3	50.8	61.0	64.2	66.4	77.0	42.2	56.8	68.1	69.6	58.1

centage points at 6-bit. Unlike ZOA, which requires bit-width-specific learning rates [4], our approach maintains constant hyperparameters across all quantization levels, demonstrating superior robustness.

### 5.3 Ablation Studies

**Computational complexity analysis.** Tab. 3 compares the wall-clock time, memory consumption and percentage of adaptation batches of PACE against BP-based and BP-free baselines. While PACE maintains the low memory footprint typical of BP-free methods, it improves efficiency over leading alternatives such as FOA and ZOA (fp=28). Specifically, our adaptation stopping technique reduces their wall-clock time by 53% and 46%, respectively, cutting runtime from over 10 h to 5.4 h while simultaneously increasing accuracy.

When we increase the threshold  $\epsilon$  to match the runtime of default ZOA (PACE with  $\epsilon \in \{0.125, 0.14\}$ ), accuracy gains diminish to levels similar to ZOA or lower. However, PACE achieves this performance by adapting to only 3.5%–4.8% of batches, requiring only a single forward pass for the remaining samples. For PACE ( $K=6$ ), we reduce the population size and maintain the default  $\epsilon$ , which outperforms ZOA by 0.3 percentage points and reduces runtime by an additional 0.1 h, despite adapting to 13.7% of batches. These results indicate that the adaptation stopping has its limits and keeping the  $\epsilon$  threshold low while decreasing population size is a more effective strategy for drastically minimizing total runtime. Notably, ZOA cannot achieve similar efficiency gains because it requires at least two forward passes per batch for gradient estimation.

**Effectiveness of PACE components.** Tab. 4 decomposes the performance gains of PACE across its three core components. To isolate the impact of subspace adaptation, we first compare PACE v1 against FOA. While both methods employ CMA-ES, FOA updates input prompts whereas PACE v1 exclusively utilizes subspace adaptation. PACE v1 outperforms FOA by 1.1 percentage points, demonstrating that the low-dimensional update of normalization layers is more effective than input prompt tuning.

**Table 3.** Computation complexity comparison on ImageNet-C with ViT-B. Forward and backward passes (#FP / #BP) are counted for processing a single sample. The wall-clock time (hours) and memory usage (MB) are measured for processing the whole ImageNet-C on a single RTX 4090 GPU. Adapted batches are indicated by the percentage on which adaptation was performed.

Method	Backprop.	#FP	#BP	Avg. Acc. (%)	Runtime (hours)	Memory (MB)	Adapt. Batches (%)
NoAdapt	✗	1	0	55.5	0.01	819	0
TENT	✓	1	1	61.7	0.03	5,165	100
SAR	✓	[1, 2]	[0, 2]	61.5	1.1	5,166	100
CoTTA	✓	3 or 35	1	58.4	1.5	16,836	100
T3A	✗	1	0	56.9	0.7	957	100
FOA	✗	28	0	65.0	11.6	832	100
ZOA	✗	2	0	61.5	0.7	858	100
ZOA (fp=28)	✗	28	0	66.3	10.0	862	100
PACE ( $\epsilon=0.125$ )	✗	1 or 28	0	61.5	0.8	863	4.8
PACE ( $\epsilon=0.14$ )	✗	1 or 28	0	61.0	0.7	863	3.5
PACE ( $K=6$ )	✗	1 or 6	0	61.8	0.6	863	13.7
PACE	✗	1 or 28	0	<b>67.0</b>	5.4	863	50.6

**Table 4.** Ablation study on each component of PACE on ImageNet-C with ViT-B.

Method	adapt. stopping	vector bank	subspace adapt.	Avg. Acc.	Runtime (hours)
NoAdapt				55.5	0.01
Baseline (FOA)				65.0	11.6
PACE v1			✓	66.1	10.3
PACE v2		✓	✓	67.2	10.3
PACE v3	✓		✓	66.3	5.4
PACE	✓	✓	✓	67.0	5.4

Integrating the vector bank and shift detection (PACE v2) further improves accuracy. This suggests that the model effectively reuses fine-tuned vectors from previously encountered similar domains. This configuration achieves the highest overall result by maintaining updates for every data point. In contrast, PACE v3 prioritizes efficiency by utilizing adaptation stopping but not the vector bank, which reduces runtime. Ultimately, the full PACE provides the optimal trade-off, combining all three components to achieve high accuracy with low computational overhead.

**Performance On Recurring Domains.** Tab. 5 compares PACE against BP-free approaches in long-term continual adaptation scenarios involving recurring domains, following [12, 21, 30]. We evaluate performance on the repeated ImageNet-C. While competing methods require multiple passes over the benchmark to converge toward our accuracy, PACE achieves a significantly high accuracy at the first round, then peaks by the second and maintains stability across

**Table 5.** Comparisons with state-of-the-art methods on ImageNet-C with ViT-B in long-term continual adaptation. We report average accuracy at each round of continual adaptation. **Bold** indicates best result, underlined second.

Method	round 1	round 2	round 3	round 4	round 5
NoAdapt	55.5	55.5	55.5	55.5	55.5
T3A	55.4	55.9	55.2	55.0	54.6
FOA	65.0	65.6	66.1	66.2	66.4
ZOA	61.5	63.0	63.2	63.9	64.0
ZOA (fp=28)	<u>66.3</u>	<u>67.4</u>	<u>67.3</u>	<u>67.8</u>	<b>68.0</b>
PACE (ours)	<b>67.0</b>	<b>67.9</b>	<b>67.8</b>	<b>68.1</b>	<u>67.8</u>

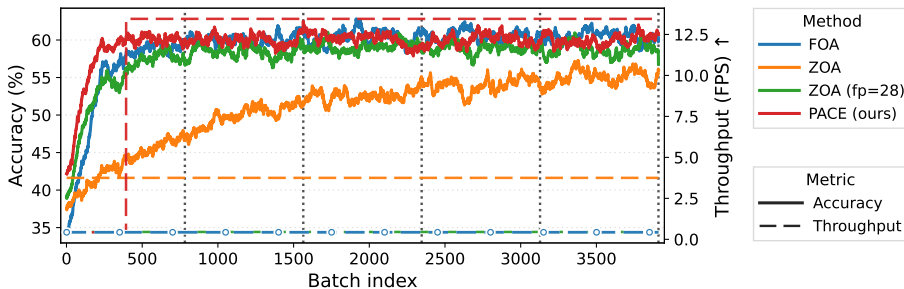


**Fig. 6.** Smoothed per-batch accuracy for the repeated *Glass Blur* domain from ImageNet-C with ViT-B model. The throughput was measured on a JETSON XAVIER NX. The gray vertical lines indicate the start of each repetition. The throughput from ZOA (fp=28) is covered by FOA.

the subsequent ones. Only ZOA (fp = 28) outperforms PACE after five repetitions, gaining a marginal 0.2 percentage points of accuracy after the fourth repetition, while adapting to all test samples. Fig. 6 illustrates per-batch accuracy and throughput for repeated *Glass Blur* domain from ImageNet-C. PACE identifies when adaptation is no longer necessary and terminates redundant updates, maintaining a throughput of 13 fps on the JETSON XAVIER NX. While FOA and ZOA (fp=28) maintain similar accuracy, they expend computational resources by adapting throughout the entire sequence, resulting in a significantly lower throughput of 0.45 fps.

## 6 Conclusions

In this work, we presented PACE, an efficient BP-free framework for continual test-time adaptation. By exploiting the low intrinsic dimensionality of normalization layer updates in TTA, PACE overcomes the restricted learning capacity of prior BP-free methods without the prohibitive memory requirements of back-propagation. Furthermore, the introduction of an adaptation stopping criterion

and a domain-specialized vector bank ensures that PACE remains efficient and robust during long-term deployment across recurring distribution shifts. Our approach enables high-performance adaptation on resource-constrained edge devices.

Empirical evaluations shows that PACE establishes a new state-of-the-art for BP-free methods. These results also suggest that high-dimensional weight optimization is not a prerequisite for effective TTA. Instead, searching low-dimensional subspaces via evolution strategies provides a viable path toward practical, on-the-fly model refinement.

## Acknowledgements

This research was funded in whole or in part by National Science Centre, Poland, grant no 2024/53/N/ST6/03156 and 2023/51/D/ST6/02846. We gratefully acknowledge Polish high-performance computing infrastructure PLGrid (HPC Center: ACK Cyfronet AGH) for providing computer facilities and support within computational grant no. PLG/2025/018634 and PLG/2025/018644. This research was funded in whole or in part by the Austrian Science Fund (FWF) 10.55776/COE12. The authors would like to thank Prof. Piotr Skrzypczyński for his valuable feedback on this paper.

## References

1. Boudiaf, M., Mueller, R., Ben Ayed, I., Bertinetto, L.: Parameter-free online test-time adaptation. In: Proceedings of the IEEE/CVF Conference on Computer Vision and Pattern Recognition. pp. 8344–8353 (2022)
2. Chen, G., Niu, S., Chen, D., Zhang, S., Li, C., Li, Y., Tan, M.: Cross-device collaborative test-time adaptation. *Advances in Neural Information Processing Systems* **37**, 122917–122951 (2024)
3. Deng, J., Dong, W., Socher, R., Li, L.J., Li, K., Fei-Fei, L.: Imagenet: A large-scale hierarchical image database. In: 2009 IEEE conference on computer vision and pattern recognition. pp. 248–255. Ieee (2009)
4. Deng, Z., Chen, G., Niu, S., Luo, H., Zhang, S., Yang, Y., Chen, R., Luo, W., Tan, M.: Test-time model adaptation for quantized neural networks. In: Proceedings of the 33rd ACM International Conference on Multimedia. pp. 7258–7267 (2025)
5. Döbler, M., Marsden, R.A., Yang, B.: Robust mean teacher for continual and gradual test-time adaptation. In: Proceedings of the IEEE/CVF Conference on Computer Vision and Pattern Recognition. pp. 7704–7714 (2023)
6. Dosovitskiy, A., Beyer, L., Kolesnikov, A., Weissenborn, D., Zhai, X., Unterthiner, T., Dehghani, M., Minderer, M., Heigold, G., Gelly, S., Uszkoreit, J., Hounsby, N.: An image is worth 16x16 words: Transformers for image recognition at scale. *ICLR* (2021)
7. Duan, D., Xu, R., Liu, P., Wen, F.: Lifelong test-time adaptation via online learning in tracked low-dimensional subspace. In: The Thirty-ninth Annual Conference on Neural Information Processing Systems (2025)

8. Gong, T., Jeong, J., Kim, T., Kim, Y., Shin, J., Lee, S.J.: Note: Robust continual test-time adaptation against temporal correlation. *Advances in Neural Information Processing Systems* **35**, 27253–27266 (2022)
9. Hansen, N.: The cma evolution strategy: A tutorial. *arXiv preprint arXiv:1604.00772* (2016)
10. Hendrycks, D., Basart, S., Mu, N., Kadavath, S., Wang, F., Dorundo, E., Desai, R., Zhu, T., Parajuli, S., Guo, M., et al.: The many faces of robustness: A critical analysis of out-of-distribution generalization. In: *Proceedings of the IEEE/CVF international conference on computer vision*. pp. 8340–8349 (2021)
11. Hendrycks, D., Dietterich, T.: Benchmarking neural network robustness to common corruptions and perturbations. *Proceedings of the International Conference on Learning Representations* (2019)
12. Hoang, T.H., Vo, M., Do, M.: Persistent test-time adaptation in recurring testing scenarios. *Advances in Neural Information Processing Systems* **37**, 123402–123442 (2024)
13. Hong, J., Lyu, L., Zhou, J., Spranger, M.: Mecta: Memory-economic continual test-time model adaptation. In: *The Eleventh International Conference on Learning Representations* (2023)
14. Iwasawa, Y., Matsuo, Y.: Test-time classifier adjustment module for model-agnostic domain generalization. *Advances in Neural Information Processing Systems* **34**, 2427–2440 (2021)
15. Jia, H., Kwon, Y., Orsino, A., Dang, T., Talia, D., Mascolo, C.: Tinytta: Efficient test-time adaptation via early-exit ensembles on edge devices. *Advances in Neural Information Processing Systems* **37**, 43274–43299 (2024)
16. Khurana, A., Paul, S., Rai, P., Biswas, S., Aggarwal, G.: Sita: Single image test-time adaptation. *arXiv preprint arXiv:2112.02355* (2021)
17. Le, Q., Sarlós, T., Smola, A., et al.: Fastfood-approximating kernel expansions in loglinear time. In: *Proceedings of the international conference on machine learning*. vol. 85 (2013)
18. Lim, H., Kim, B., Choo, J., Choi, S.: Ttn: A domain-shift aware batch normalization in test-time adaptation. *arXiv preprint arXiv:2302.05155* (2023)
19. Mirza, M.J., Masana, M., Possegger, H., Bischof, H.: An efficient domain-incremental learning approach to drive in all weather conditions. In: *Proceedings of the IEEE/CVF Conference on Computer Vision and Pattern Recognition*. pp. 3001–3011 (2022)
20. Nado, Z., Padhy, S., Sculley, D., D’Amour, A., Lakshminarayanan, B., Snoek, J.: Evaluating prediction-time batch normalization for robustness under covariate shift. *arXiv preprint arXiv:2006.10963* (2020)
21. Niu, S., Miao, C., Chen, G., Wu, P., Zhao, P.: Test-time model adaptation with only forward passes. In: *The International Conference on Machine Learning* (2024)
22. Niu, S., Wu, J., Zhang, Y., Chen, Y., Zheng, S., Zhao, P., Tan, M.: Efficient test-time model adaptation without forgetting. In: *ICML*. vol. 162, pp. 16888–16905 (2022)
23. Niu, S., Wu, J., Zhang, Y., Wen, Z., Chen, Y., Zhao, P., Tan, M.: Towards stable test-time adaptation in dynamic wild world. In: *International Conference on Learning Representations* (2023)
24. Peng, X., Bai, Q., Xia, X., Huang, Z., Saenko, K., Wang, B.: Moment matching for multi-source domain adaptation. In: *Proceedings of the IEEE/CVF international conference on computer vision*. pp. 1406–1415 (2019)

25. Schneider, S., Rusak, E., Eck, L., Bringmann, O., Brendel, W., Bethge, M.: Improving robustness against common corruptions by covariate shift adaptation. *Advances in neural information processing systems* **33**, 11539–11551 (2020)
26. Spall, J.C.: Multivariate stochastic approximation using a simultaneous perturbation gradient approximation. *IEEE transactions on automatic control* **37**(3), 332–341 (2002)
27. Sun, Y., Wang, X., Liu, Z., Miller, J., Efros, A., Hardt, M.: Test-time training with self-supervision for generalization under distribution shifts. In: *International conference on machine learning*. pp. 9229–9248. PMLR (2020)
28. Tan, M., Chen, G., Wu, J., Zhang, Y., Chen, Y., Zhao, P., Niu, S.: Uncertainty-calibrated test-time model adaptation without forgetting. *IEEE Transactions on Pattern Analysis and Machine Intelligence* (2025)
29. Touvron, H., Cord, M., Douze, M., Massa, F., Sablayrolles, A., Jegou, H.: Training data-efficient image transformers & distillation through attention. In: Meila, M., Zhang, T. (eds.) *Proceedings of the 38th International Conference on Machine Learning. Proceedings of Machine Learning Research*, vol. 139, pp. 10347–10357. PMLR (18–24 Jul 2021), <https://proceedings.mlr.press/v139/touvron21a.html>
30. Vray, G., Tomar, D., Gao, X., Thiran, J.P., Shelhamer, E., Bozorgtabar, B.: Reservoirtta: Prolonged test-time adaptation for evolving and recurring domains. *arXiv preprint arXiv:2505.14511* (2025)
31. Wang, D., Shelhamer, E., Liu, S., Olshausen, B., Darrell, T.: Tent: Fully test-time adaptation by entropy minimization. In: *International Conference on Learning Representations* (2021), <https://openreview.net/forum?id=uX13bZLkr3c>
32. Wang, Q., Fink, O., Van Gool, L., Dai, D.: Continual test-time domain adaptation. In: *Proceedings of the IEEE/CVF conference on computer vision and pattern recognition*. pp. 7201–7211 (2022)
33. Wightman, R.: Pytorch image models. <https://github.com/rwightman/pytorch-image-models> (2019). <https://doi.org/10.5281/zenodo.4414861>
34. Yuan, Z., Xue, C., Chen, Y., Wu, Q., Sun, G.: Ptq4vit: Post-training quantization for vision transformers with twin uniform quantization. In: *European conference on computer vision*. pp. 191–207. Springer (2022)
35. Zhang, Y., Gong, K., Ding, X., Zhang, K., Lv, F., Keutzer, K., Yue, X.: Towards unified and effective domain generalization (2023)
36. Zhao, B., Chen, C., Xia, S.T.: Delta: degradation-free fully test-time adaptation. *arXiv preprint arXiv:2301.13018* (2023)

## Appendix

### A.1 Overview

This Appendix provides comprehensive implementation details (Sec. A.2) and additional experiments (Sec. A.3). Experiments include the ablation studies (Sec. A.3.1) on the optimization dimensionality  $d$ , capacity of domain-specialized vector bank  $p$ , and domain shift threshold  $\gamma$ . Moreover, Sec. A.3.2 includes detailed results on the ImageNet-C benchmark.

### A.2 Implementation Details

We adopt the hyperparameter settings specified in the original papers for all baselines, except where they were not provided. In those instances, the learning rate was specifically tuned for our model and experimental setup. We utilized method implementations from the code repository of FOA [21] and ZOA [4]. In the following, we present the details regarding each method.

**PACE (ours)**. To ensure a fair comparison with FOA, we configure the CMA-ES population size  $K$  to 28 and set the optimization vector dimensionality  $d$  to 2304. Following FOA and ZOA, we utilize the validation set of ImageNet-1K to compute the statistics of in-distribution data, setting  $\lambda$  to 0.2 for ImageNet-R and 0.4 for all other benchmarks. We set the domain shift detection threshold  $\gamma$  to 0.03, the adaptation stopping threshold  $\epsilon$  to 0.045, and the maximum capacity of the domain-specialized vector buffer  $p$  to 30. Our method specifically updates the affine parameters of the normalization layers. Following ZOA, we keep the layer normalization parameters of the first block and the last three blocks of the tested models fixed.

**FOA** [21]. We set the number of input prompt embeddings to 3 and the population size  $K$  to 28. In-distribution statistics are computed using the ImageNet-1K validation set. The loss trade-off parameter  $\lambda$  is set to 0.2 for ImageNet-R and 0.4 for all other benchmarks, while the moving average factor for batch-to-source shift activation is maintained at 0.1.

**ZOA** [4]. The learnable parameters are perturbed with a step size of 0.02 for gradient estimation, while the step size for the coefficients of different domain parameters is set to 0.05. The SGD optimizer with a weight decay of 0.4 is used to update the model parameters, and the AdamW optimizer with a weight decay of 0.1 is used to update the coefficients. The maximum number of domain knowledge parameters is set to 32. The learning rate for coefficients is set to 0.01 for all setups. The learning rate for model parameters is set to 0.0002 for 6-bit ViT-B and 0.0005 for all other models. In terms of ZOA ( $fp=28$ ), the optimal learning rate chosen on ImageNet-C is set to 0.005 for all models and datasets.

**LAME** [1]. Following [21], we use the kNN affinity matrix set to 5, as this value was found to be optimal for ImageNet-C.

**T3A** [14]. Following [21], the number of supports to restore  $M$  is set to 20, as this value was found to be optimal for ImageNet-C.

**TENT** [31]. We use SGD optimizer, with a momentum of 0.9. The learning rate was tuned on ImageNet-C and set to 0.0001 for both ViT-B and DeiT-B models. **SAR** [23]. We use SGD optimizer with a momentum of 0.9. The learning rate tuned on ImageNet-C is set to 0.001 for both ViT-B and DeiT-B. The entropy threshold  $E_0$  is set to  $0.4 \times \ln C$ , where C is the number of task classes. **CoTTA** [32]. We use SGD optimizer, with a momentum of 0.9. The learning rate was tuned on ImageNet-C and set to 0.001 for ViT-B and 0.005 for DeiT-B. The augmentation threshold  $p_{th}$  is set to 0.1. The restoration probability is set to 0.01 and the EMA factor for teacher update is set to 0.999.

### A.3 Additional Experimental Results

#### A.3.1 Ablation Studies

**Optimization dimensionality ( $d$ ).** Tab. A.1 (a) shows performance degradation when  $d$  is either increased or decreased. The reduction in accuracy at lower dimensions indicates insufficient expressivity for the optimization updates. Meanwhile, the drop at higher dimensions is likely due to the increased search space complexity, which would require a larger CMA-ES population than our budget of 28.

**Domain-Specialized Vector Bank maximum capacity ( $p$ ).** Tab. A.1 (b) shows the impact of the domain-specialized vector bank capacity  $p$  on the ImageNet-C benchmark. Performance improves as  $p$  increases, reaching a plateau at  $p=15$ . This behavior is expected since ImageNet-C consists of 15 distinct domains. As shown in Fig. A.1, our method successfully detects almost every domain transition and initializes from the bank (see Throughput). Consequently, increasing the capacity beyond the number of available domains yields no further gains.

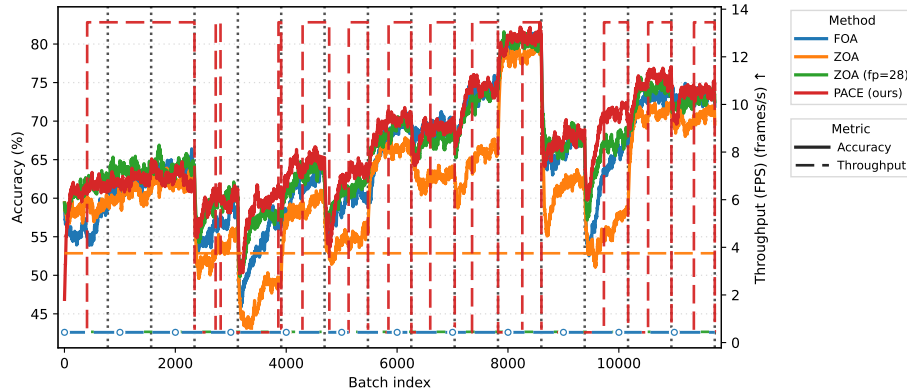
**Domain shift threshold  $\gamma$ .** The effect of domain shift threshold  $\gamma$  is evaluated in Tab. A.1 (c). While a lower  $\gamma$  increases sensitivity to distribution shifts, frequent resets prevent the CMA-ES from reaching an optimal distribution. On the other hand, a higher  $\gamma$  results in insufficient sensitivity, leaving the model with suboptimal starting points when significant shifts occur. Our results suggest that a balanced threshold is necessary to maintain both detection accuracy and optimization stability.

#### A.3.2 Detailed ImageNet-C Results

Fig. A.1 illustrates the per-batch accuracy and throughput on the ImageNet-C dataset using a JETSON XAVIER NX. PACE dynamically leverages throughput by prioritizing adaptation at the onset of new domains (resulting in temporary throughput drops) and resuming high-speed inference once the domain stabilizes. In contrast, competing approaches maintain significantly lower throughput while achieving inferior accuracy (see Tab. A.2). While certain domain shifts remain undetected due to inter-domain similarity, this suggests that re-initiating adaptation in such instances is unnecessary.

**Table A.1.** Accuracy (%) of PACE on ImageNet-C with a ViT-B model.

(a) low-dimension space ( $d$ )						
	300	768	2304	3000		
PACE (ours)	63.8	65.4	<b>67.0</b>	66.5		
(b) maximum vector bank capacity ( $p$ )						
	0	5	15	30	40	50
PACE (ours)	66.3	66.6	<b>67.0</b>	<b>67.0</b>	<b>67.0</b>	<b>67.0</b>
(c) domain shift threshold ( $\gamma$ )						
	0.01	0.02	0.03	0.05	0.1	1.5
PACE (ours)	65.9	<b>67.0</b>	<b>67.0</b>	66.5	66.6	63.0

**Fig. A.1.** Smoothed per-batch accuracy for the ImageNet-C benchmark with ViT-B model. The throughput was measured on JETSON XAVIER NX. The gray vertical lines indicate the start of a domain.**Table A.2.** Comparisons with SOTA methods on ImageNet-C with ViT-B regarding Accuracy (%). BP is short for backward propagation.

Method	BP	Noise			Blur			Weather				Digital			Avg.		
		Gauss.	Shot	Impul.	Defoc.	Glass	Motion	Zoom	Snow	Frost	Fog	Brit.	Contr.	Elas.		Pix.	JPEG
NoAdapt	✗	56.8	56.8	57.5	46.9	35.6	53.1	44.8	62.2	62.5	65.7	77.7	32.6	46.0	67.0	67.6	55.5
TENT	✓	57.6	59.8	60.9	51.2	49.4	59.6	53.2	64.0	62.7	67.8	78.6	66.5	54.5	70.0	69.7	61.7
CoTTA	✓	57.4	58.4	59.7	47.5	38.3	54.9	47.3	62.4	63.4	69.9	77.8	54.3	47.8	68.0	68.6	58.4
SAR	✓	59.1	61.1	61.6	54.2	55.1	58.6	55.7	60.3	61.5	64.3	76.6	58.2	58.1	68.6	68.9	61.5
LAME	✗	56.5	56.5	57.2	46.4	34.7	52.7	44.2	58.4	61.6	63.1	77.4	24.7	44.6	66.6	67.2	54.1
T3A	✗	56.4	56.6	56.7	45.5	34.4	51.9	43.4	60.6	62.8	60.9	77.1	45.8	44.5	66.7	68.5	55.4
FOA	✗	56.3	61.7	63.9	56.1	53.3	61.4	58.9	67.5	69.1	73.0	80.2	65.9	62.1	72.5	73.0	65.0
ZOA	✗	58.6	60.5	62.3	52.9	46.7	58.8	54.2	66.0	62.7	64.5	78.8	60.6	55.4	70.9	70.3	61.5
ZOA ( $fp=28$ )	✗	61.3	63.7	64.1	58.8	56.1	62.8	60.5	68.5	67.4	72.1	80.2	66.9	65.4	73.7	72.6	66.3
PACE (ours)	✗	61.2	62.3	62.7	59.1	58.2	64.2	61.3	69.6	68.4	73.5	80.7	67.1	68.7	74.9	73.3	<b>67.0</b>